JOURNAL OF SOLID STATE CHEMISTRY 114, 491–498 (1995)

A Thermogravimetric Study of the Influence of Internal Stresses on Oxygen Variations in $Ln_{2-x}Ce_xCuO_4$

Y. T. Zhu and A. Manthiram[1]

Center for Materials Science and Engineering, ETC 9.104, The University of Texas at Austin, Austin, Texas 78712

Received April 20, 1994; in revised form June 9, 1994; accepted June 15, 1994

The variation with temperature of oxygen content in the electron-doped superconductors $Ln_{2-x}Ce_xCuO_4$ (Ln = lanthanide) have been investigated systematically by thermogravimetric analysis. The tendency to lose oxygen generally decreases with increasing Ce content or decreasing Ln^{3+} size due to a decreasing degree of internal stresses resulting from an improved bond length matching between the (Ln, Ce)–O and Cu–O bonds; this is supported by bond valence sum calculations. With smaller a lattice parameters as in $Gd_{2-x}Ce_xCuO_4$, however, an increasing electrostatic repulsion between the interstitial octahedral-site and the normal tetrahedral-site oxygen atoms forces the excess interstitial oxygen atoms to be lost at lower temperatures. It also causes the oxygen loss to occur in two steps, one corresponding to the interstitial oxygen and the other to the tetrahedral-site oxygen atoms. In contrast, the oxygen loss occurs smoothly in one step for larger a lattice parameters as in $LaNd_{1-x}Ce_xCuO_4$.

1. INTRODUCTION

Copper oxide superconductors have intergrowth structures in which CuO_2 sheets alternate with other A_xO_y (A = alkaline earth or lanthanide) layers along the c-axis. The stabilization of such structures requires bond length matching between the Cu–O and A–O bonds (1, 2). Any bond length mismatch will result in a buildup of internal stresses and may have important consequences: For example, the p- vs n-type doping in the Ln_2CuO_4 (Ln = lanthanide) oxides is determined by the type of internal stresses—compressive vs tensile—as pointed out by Goodenough (1). The internal stresses influence the distribution of charges between the $Cu(1)O_x$ and $Cu(2)O_2$ layers in $YBa_2Cu_3O_{6+x}$ phases (3, 4). The variation of the environmental reactivity of $YBa_2Cu_3O_{6+x}$ phases with the oxygen content has also been correlated to the internal stresses (5).

The electron-doped superconductors $Ln_{2-x}Ce_xCuO_4$ have CuO_2 sheets alternating with the $Ln_{2-x}Ce_xO_2$ fluorite layers (Fig. 1). Direct electrostatic repulsion between the negatively charged O^{2-} ions of the fluorite Ln–O_2–Ln layers increases the a lattice parameter, which results in a tensile stress in the Cu–O bonds and a compressive stress in the Ln–O bonds (1, 2). It is the tensile stress in the Cu–O bonds of the T′ structure which makes the n-type doping readily feasible and the p-type doping difficult.

The degree of bond length mismatch and the magnitude of internal stresses decrease as the Ln^{3+} size in $Ln_{2-x}Ce_xCuO_4$ decreases. From a systematic variation through Ln^{3+} size of the a lattice parameter, we have shown recently (6) that a decreasing tensile stress in the Cu–O bonds causes a monotonic decrease in the Ce solubility limit in $Ln_{2-x}Ce_xCuO_4$ as the size of the Ln^{3+} ion decreases. We also showed from wet-chemical analysis that the decreasing tensile stress causes a decrease in the ease with which oxygen vacancies can be created. For a given N_2-annealing temperature, the oxygen content increases—i.e., the oxygen vacancy concentration decreases—with decreasing size of Ln^{3+} ions or increasing Ce concentration in $Ln_{2-x}Ce_xCuO_4$. The decreasing oxygen concentration necessitates a higher critical Ce concentration x_c to induce the transition from antiferromagnetic semiconductor to superconductor as the size of Ln^{3+} decreases, although the transition occurs at a fixed critical electron concentration $n_c = 0.175 + 0.005$ irrespective of the Ln^{3+} size. We show in this paper from thermogravimetric analysis (TGA) data how the internal stresses caused by bond length mismatch in $Ln_{2-x}Ce_xCuO_4$ influence the variation of oxygen content and phase stability in N_2 atmospheres at higher temperatures.

2. EXPERIMENTAL

The $Ln_{2-x}Ce_xCuO_4$ samples for Ln = $La_{1-y}Nd_y$, Nd, Sm, and Eu were prepared by a coprecipitation technique (6–8). Required quantities of predried Ln_2O_3, ceric ammonium nitrate, and Cu metal were dissolved in dilute nitric acid, and the metal ions were coprecipitated as carbonates by adding potassium carbonate until the pH rose to 7. The coprecipitate was washed with water, dried at 100°C,

[1] To whom correspondence should be addressed.

0022-4596/95 $6.00

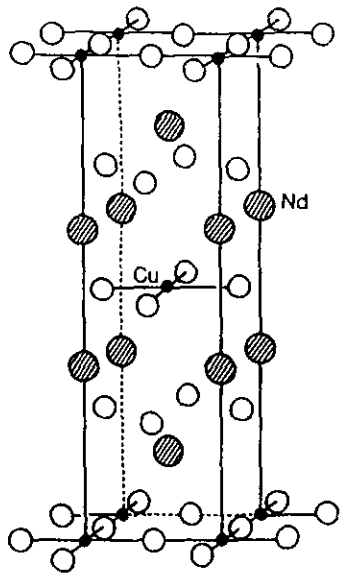

FIG. 1. Crystal structure of T' Nd_2CuO_4.

and fired at 500°C for 6 hr. The resulting black powder was ground, pelletized, and refired at 1000°C for 48 hr with one intermittent grinding. $Ln_{2-x}Ce_xCuO_4$ samples for Ln = Gd and $Gd_{1-y}Dy_y$ were synthesized by conventional solid state procedures by firing required quantities of Ln_2O_3, CeO_2, and CuO first at 900°C for 20 hr and then at 1050°C for 48 hr with one intermittent grinding. In both the cases, the samples were allowed to cool in the furnace by turning off the power after the final firing schedule. The samples so obtained were characterized by X-ray powder diffraction.

TGA plots were recorded with a Perkin–Elmer Series 7 thermal analysis system in N_2 atmosphere. A baseline was first recorded with the empty platinum crucible under conditions identical to that employed for the samples. The baseline was then used for correcting the curves recorded with the samples to avoid any error arising from buoyancy or the instrument. The TGA curves were recorded by loading about 100 mg of powdered sample into the platinum crucible. The noise level is much less than 0.005 mg, which corresponds to an error of <0.005%. In addition, the samples were all stored in a desiccator immediately after synthesis and were removed from the desiccator just before the TGA experiment. They were all purged with N_2 at 100°C in the TGA instrument for about 2 hr before recording the plot. These precautions were taken to avoid any error that may add to the weight loss due to the absorbed/adsorbed moisture and other species from the ambient. With careful experimentation, the % weight losses were found to be reproducible within ±0.005%. The products obtained after the TGA experiments were characterized by X-ray diffraction to detect phase decomposition and to identify the phases.

In order to understand the effect of the heating rate on the observed results, TGA experiments were first carried out with different heating rates of 1, 2, 5, and 10°C/min for $LaNd_{1-x}Ce_xCuO_4$ samples with $x = 0.10$ and 0.14. The % weight loss at a given temperature was found to be nearly the same (within ±0.005%) for all heating rates of ≤5°C/min; the heating rate of 10°C/min showed smaller weight loss than that found with ≤5°C/min. Therefore, a slow heating rate of 1°C/min was employed uniformly for all the samples investigated in this paper to avoid variations that could otherwise arise from kinetic effects. Furthermore, no additional weight loss was found to occur upon maintaining a sample of $LaNd_{0.9}Ce_{0.1}CuO_4$ isothermally for several hours at 900°C, after heating it from 100 to 900°C at a heating rate of 1°C/min. These experiments reveal that the results presented are not influenced by any adverse kinetic factor.

3. RESULTS AND DISCUSSION

3.1. $LaNd_{1-x}Ce_xCuO_4$ Phases

The T' structure is stabilized for $0.09 \leq x \leq 0.24$ in $LaNd_{1-x}Ce_xCuO_4$ (6, 9, 10). For $x < 0.09$, T phase impuri-

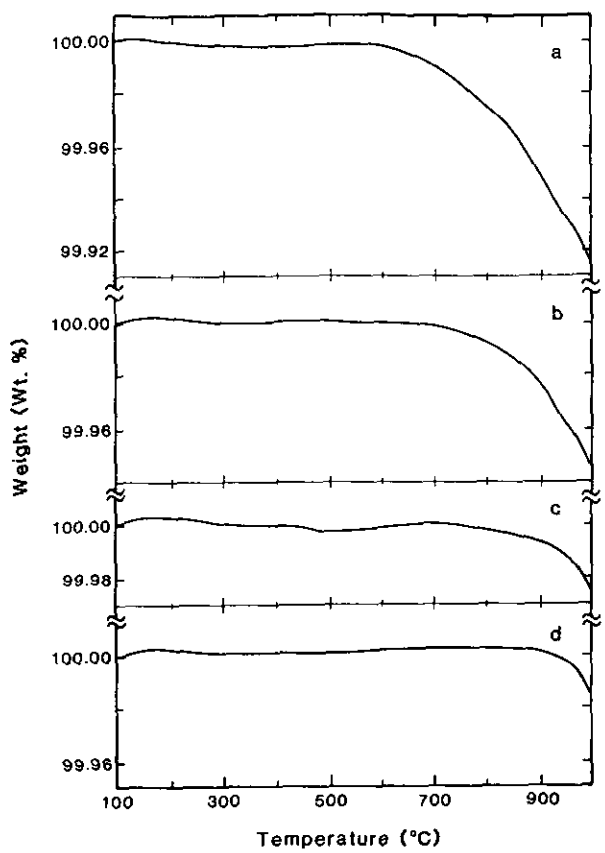

FIG. 2. TGA plots recorded in N_2 atmosphere for $LaNd_{1-x}Ce_xCuO_4$: (a) $x = 0.10$, (b) $x = 0.14$, (c) $x = 0.18$, and (d) $x = 0.23$.

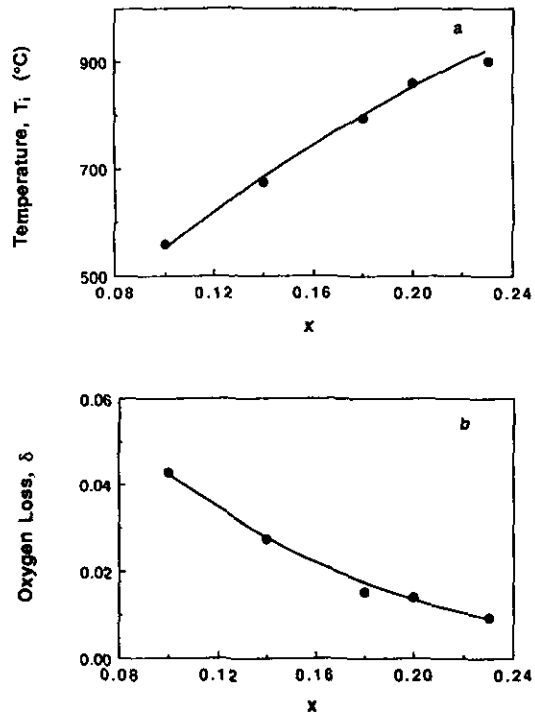

FIG. 3. Variation with x of (a) the temperature T_i at which oxygen loss begins and (b) the amount of oxygen lost at 1000°C in N_2 atmosphere for $LaNd_{1-x}Ce_xCuO_4$.

ties are formed. This system is near the upper limit of the T′ phase field and any increase in the average size of Ln^{3+}—by either an increase in La^{3+} concentration or a decrease in Ce content x—leads to the formation of T phase impurities. A larger average Ln^{3+} size in $LaNd_{1-x}Ce_xCuO_4$ increases the Ce solubility to 0.24 compared to a Ce solubility of 0.20 in $Nd_{2-x}Ce_xCuO_4$. The TGA plots of $LaNd_{1-x}Ce_xCuO_4$ recorded in N_2 atmosphere under identical conditions are shown in Fig. 2 for different values of x. The observed weight loss at higher temperatures is due to oxygen loss. The as-prepared $Ln_{2-x}Ce_xCuO_{4+\delta}$ samples all have $0 < \delta \leq 0.02$ excess oxygen atoms as revealed by iodometric titration (6, 11). Other groups have also found excess oxygen atoms in the as-prepared samples from iodometric analysis (12, 13) or TGA analysis (14). The excess oxygen atoms presumably occupy the empty octahedral interstitial sites within the $(Ln, Ce)_2O_2$ fluorite layers. These interstitial atoms are stable to at least 500°C. At higher temperatures, these interstitial oxygen atoms along with some additional oxygen atoms from the tetrahedral sites of the $(Ln, Ce)_2O_2$ fluorite layer are lost to give $Ln_{2-x}Ce_xCuO_{4-\delta}$.

The temperature T_i at which oxygen loss begins increases with increasing Ce-doping x as shown in Fig. 3a. The amount of oxygen lost per $LaNd_{1-x}Ce_xCuO_4$ formula unit at 1000°C decreases with increasing x as shown in Fig. 3b. A similar trend is also found in previous investigations of the system $Nd_{2-x}Ce_xCuO_4$ (14, 15). The results of Fig. 3 show that the removal of oxygen becomes increasingly difficult as the value of x increases, which is in agreement with the trend obtained from iodometric analysis data (6, 11–13). The oxygen content obtained from iodometric titration after annealing the $LaNd_{1-x}Ce_xCuO_4$ samples at a constant temperature T = 950°C in N_2 atmosphere for 20 hr increases with increasing Ce content (6, 11).

The decreasing tendency to lose oxygen with increasing Ce content can be understood on the basis of the internal stresses introduced by bond length mismatch. The strain arising from the internal stresses can be estimated using the bond valence sum (BVS) model (3, 4). In the BVS model, the bond valence s is calculated as

$$s = \exp[(R_0 - R)/B], \quad [1]$$

where R is the equilibrium bond length and R_0 and B are constants. The values of R_0 and B have been tabulated for several bond types (16). For most inorganic compounds, the sum of the bond valences around a given atom lies within 0.1 of its formal oxidation state (17) and the BVS model can be used to obtain the oxidation states in systems having mixed oxidation states (18, 19) such as $YBa_2Cu_3O_{6+x}$ (3, 20–22). In the T′ $Ln_{2-x}Ce_xCuO_4$, the Cu atoms have square-coplanar oxygen coordination and the bond valence sum V at the Cu atom becomes

$$V = 4s = 4\exp[(R_0 - R)/B]. \quad [2]$$

Rearrangement of Eq. [2] gives the equilibrium bond length R expected from BVS for a given valence state V as

$$R = R_0 - B\ln(V/4). \quad [3]$$

Comparison of the equilibrium bond length obtained

TABLE 1
Calculation of Strain in $LaNd_{1-x}Ce_xCuO_{4.015}$

x	Formal Cu valence	Cu–O bond length (Å)		ΔR (Å)[c]	Strain (%)[d]
		Measured[a]	BVS[b]		
0.10	*1.93*	*1.9897*	*1.943*	*0.0467*	*2.40*
0.14	1.89	1.9896	1.948	0.0416	2.15
0.18	1.85	1.9902	1.953	0.0372	1.93
0.20	1.83	1.9903	1.955	0.0353	1.81
0.23	1.80	1.9905	1.959	0.0315	1.62

[a] Obtained from measured lattice parameter as $R_{Cu-O} = a/2$.
[b] Calculated based on bond valence sum (BVS) using Eq. [3].
[c] Difference between measured and calculated Cu–O bond lengths.
[d] Obtained as (ΔR/BVS Cu–O bond length) × 100.

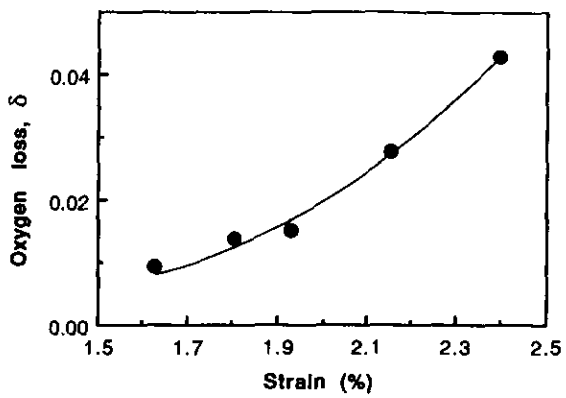

FIG. 4. Variation of the amount of oxygen lost at 1000°C in N_2 atmosphere with the strain in the Cu–O bond for $LaNd_{1-x}Ce_xCuO_4$. The strain was calculated using bond valence sum method.

from Eq. [3] with that obtained from the measured lattice parameter can provide an estimate of the strain present in the Cu–O bond. The values obtained by such a procedure for $LaNd_{1-x}Cu_xCuO_{4.015}$ are given in Table 1. The values of B and R_0 in Eq. 3 were taken as provided by Brown (3): $B = 0.37$, and $R_0 = 1.679$ Å for the Cu^{2+}–O^{2-} bond and 1.60 Å for the Cu^{+}–O^{2-} bond. For intermediate oxidation states between Cu^{2+} and Cu^{+}, a weighted average of the R_0 values for Cu^{2+} and Cu^{+} were used. The as-prepared $LaNd_{1-x}Ce_xCuO_{4+\delta}$ samples all had a $\delta = 0.015 \pm 0.005$, and an oxygen content of 4.015 was used for all the samples in computnig the formal valence V of Cu. The measured Cu–O bond lengths are larger than the expected BVS values, which indicates that the Cu–O bonds are under a tensile stress. The calculated % tensile strain is given in the last column of Table 1. The difference ΔR_{Cu-O} between the expected and measured Cu–O bond lengths and the % strain decrease with increasing Ce content.

Creation of oxygen vacancies in $Ln_{2-x}Ce_xCuO_{4-\delta}$ will introduce antibonding electrons into the CuO_2 sheets, which can relieve the tensile stress in the Cu–O bonds. Also, oxygen vacancies in the (Ln, Ce)$_2O_{2-\delta}$ fluorite layer will reduce the electrostatic repulsion between the O^{2-} ions, which may tend to relieve slightly the compressive stress in the (Ln, Ce)–O bonds. As the Ce content in $LaNd_{1-x}Ce_xCuO_4$ increases, the bond length mismatch and the degree of internal stresses or strain (Table 1) decrease, which results in a decreasing driving force for the acceptance of antibonding electrons and creation of oxygen vacancies. This is reflected in a decrease in T_i and oxygen loss (Fig. 3) with Ce content x. The variation of the amount of oxygen lost at 1000°C with the Cu–O bond strain is shown in Fig. 4. Closer to the solubility limit $x \approx 0.23$ in $LaNd_{1-x}Ce_xCuO_4$, it becomes increasingly difficult to create oxygen vacancies due to a decreasing internal stress.

The concentration of Cu^{+} increases with increasing Ce content in $Ln_{2-x}Ce_xCuO_4$. Since Cu^{+} generally prefers linear or tetrahedral oxygen coordination, it may be difficult to keep large concentrations of Cu^{+} in square-coplanar coordination. Although one can argue that an increasing Cu^{+} concentration with increasing Ce content may make it increasingly difficult to create additional Cu^{+} via the creation of oxygen vacancies, we will see in the next section that such a consideration could not account for the variation of oxygen contents with Ln^{3+} size for a constant Ce content. The results discussed below will show that the internal stresses play the primary role.

3.2. $Ln_{1.85}Ce_{0.15}CuO_4$ Phases

We have monitored the variation of oxygen loss with the size of Ln^{3+} for a given Ce content. The TGA plots of $Ln_{1.85}Ce_{0.15}CuO_4$ recorded in N_2 atmosphere are shown in Fig. 5 for different Ln^{3+} ions. The temperature T_i at which oxygen loss begins increases from 740°C in $LaNd_{0.85}Ce_{0.15}CuO_4$ to 800°C in $Nd_{1.85}Ce_{0.15}CuO_4$. Also the amount of oxygen loss per formula unit at 1000°C decreases from 0.028 in the former to 0.017 in the latter. The increasing difficulty of removing oxygen with decreasing Ln^{3+} size is in agreement with the results obtained from iodometric analysis of $Nd_{2-y-0.12}La_yCe_{0.12}CuO_4$ (6). The observed trend can be understood to be due to the decreasing degree of bond length mismatch and internal stresses with decreasing size of Ln^{3+} ions. The tensile strain in the Cu–O bond decreases with decreasing Ln^{3+} size (Table 2).

However, the above trend does not seem to prevail beyond Ln = Nd. Nearly the same $T_i \approx 800$°C is found for Ln = Nd and Sm, and an even lower $T_i \approx 750$°C is found for Ln = Eu and Gd. Also, the oxygen loss is found to occur in two distinct steps for Ln = Eu and Gd unlike a smooth single-step loss for Ln = (La, Nd), Nd, and Sm. The first sharp weight loss for Ln = Eu and Gd in the temperature range $750 \leq T \leq 800$°C corresponds to an oxygen loss of about 0.01 per formula unit. The second smooth drop for Ln = Eu in the temperature range $800 \leq T \leq 980$°C corresponds to an oxygen loss of 0.01 per formula unit whereas that for Ln = Gd in the range $800 \leq T \leq 920$°C corresponds to 0.005 oxygen. The third sharp drop in both cases corresponds to a decomposition of the $Ln_{2-x}Ce_xCuO_4$ phases to Ln_2O_3, CeO_2, and Cu_2O as revealed by X-ray diffraction (Fig. 6).

The unexpectedly lower $T_i \approx 750$°C found for Ln = Eu and Gd can be explained by considering the electrostatic repulsion between the O^{2-} ions. The smaller Eu^{3+} and Gd^{3+} ions lead to a lower a lattice parameter, which causes a decrease in the distance $a/\sqrt{2}$ between the oxygen atoms in the tetrahedral sites of the fluorite layer as well as the distance $\sqrt{6}\,a/4$ between the oxygen atoms in the

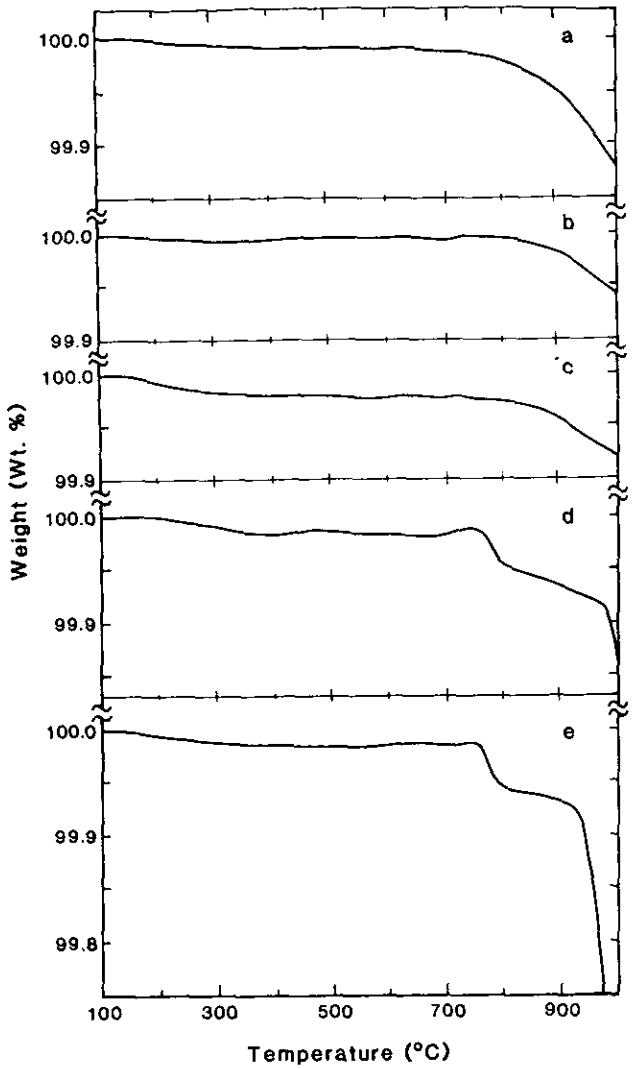

FIG. 5. TGA plots recorded in N_2 atmosphere for $Ln_{1.85}Ce_{0.15}CuO_4$: (a) $LaNd_{0.85}Ce_{0.15}CuO_4$, (b) $Nd_{1.85}Ce_{0.15}CuO_4$, (c) $Sm_{1.85}Ce_{0.15}CuO_4$, (d) $Eu_{1.85}Ce_{0.15}CuO_4$, and (e) $Gd_{1.85}Ce_{0.15}CuO_4$.

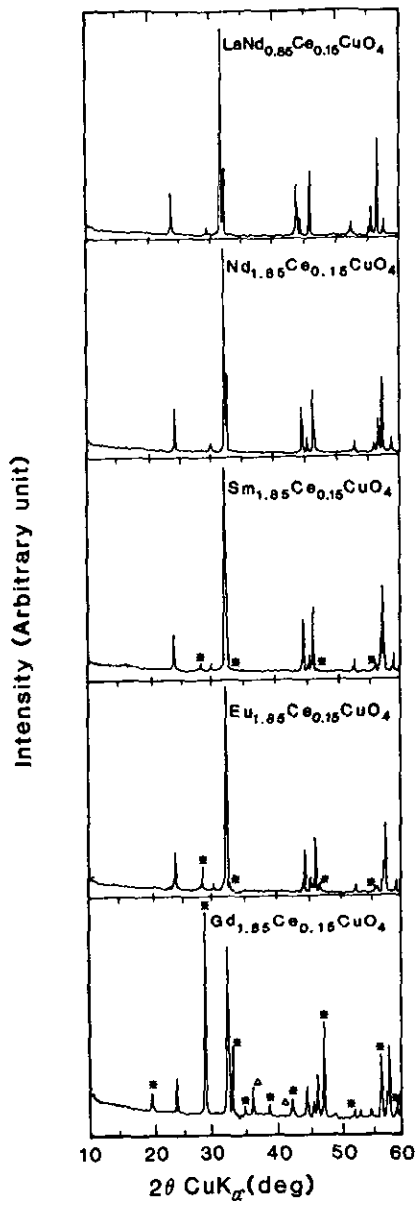

FIG. 6. X-ray diffraction patterns of the products obtained after performing TGA experiment with the $Ln_{1.85}Ce_{0.15}CuO_4$ samples in N_2 atm to 1000°C. The unmarked reflections all refer to undecomposed $Ln_{2-x}Ce_xCuO_4$; Δ refers to Cu_2O; * refers to CeO_2 or a mixture of CeO_2 and Gd_2O_3 (or Eu_2O_3), which have overlapping d values.

TABLE 2
Calculation of Strain in $Ln_{1.85}Ce_{0.15}CuO_{4.015}$

Ln	Formal Cu valence	Cu–O bond length (Å)			
		Measured[a]	BVS[b]	ΔR (Å)[c]	Strain (%)[d]
$La_{0.54}Nd_{0.46}$[e]	1.88	1.9900	1.949	0.0410	2.11
Nd	1.88	1.9734	1.949	0.0244	1.25
Gd	1.88	1.9500	1.949	0.0010	0.05

[a] Obtained from measured lattice parameter as $R_{Cu-O} = a/2$.
[b] Calculated based on bond valence sum (BVS) using Eq. [3].
[c] Difference between measured and calculated Cu–O bond lengths.
[d] Obtained as (ΔR/BVS Cu–O bond length) × 100.
[e] Corresponds to $LaNd_{1.85}Ce_{0.15}CuO_{4.015}$.

tetrahedral sites and octahedral interstitial sites. For example, $Gd_{1.85}Ce_{0.15}CuO_4$ has a lattice parameter $a = 3.902$ Å (23), which corresponds to a distance of 2.76 Å between the tetrahedral oxygen atoms and 2.39 Å between the tetrahedral- and octahedral-site oxygen atoms. The decreasing oxygen–oxygen distance with decreasing size of Ln^{3+} ion increases the electrostatic repulsion between the tetrahedral- and octahedral-site oxygen atoms, which forces the octahedral interstitial oxygen atoms to be lost

first at a lower temperature $750 \leq T \leq 800°C$. A loss of about 0.01 oxygen atoms per formula unit in the first step presumably corresponds to this. The smooth loss occurring thereafter in the second step at $T > 800°C$ corresponds to the removal of oxygen atoms from the tetrahedral sites. A decrease in the removal of tetrahedral-site oxygen atoms from 0.01 for Ln = Eu to 0.005 for Ln = Gd before decomposition occurs is in accordance with a decreasing tensile strain in the Cu–O bond with decreasing size of Ln^{3+} ion (Table 2). A relief of nearly all the tensile stress in $Gd_{1.85}Ce_{0.15}CuO_{4-\delta}$ results in an inability to sustain oxygen vacancies beyond $\delta > 0.005$ as indicated by phase decomposition.

A decreasing internal stress leads to an increasing inability to sustain oxygen vacancies with decreasing size of Ln^{3+}. This is reflected in the phase decomposition temperatures of $Ln_{1.85}Ce_{0.15}CuO_4$ in N_2 atm. The phase decomposition becomes more and more severe as the size of Ln^{3+} decreases. Accordingly, the decomposition occurs at about 920°C for Ln = Gd, and at about 980°C for Ln = Eu. No decomposition is observed for Ln = (La, Nd) and Nd at $T \leq 1000°C$. The decomposition appears to just begin at 1000°C for Ln = Sm as shown by the traces of CeO_2 impurity in the X-ray diffraction pattern (Fig. 6). An X-ray diffraction analysis of the products obtained after performing the TGA experiment at 1000°C reveals that the amount of decomposition products increases with decreasing size of Ln^{3+} ion.

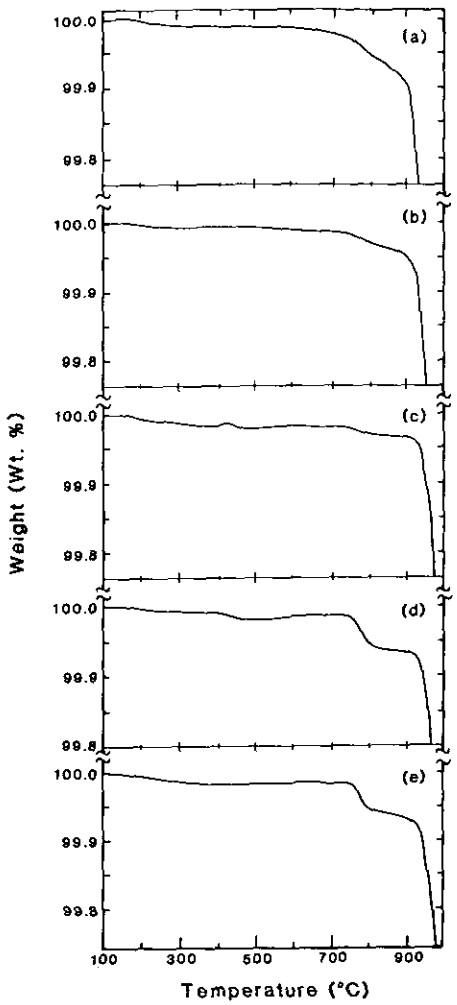

FIG. 7. TGA plots recorded in N_2 atmosphere for $Gd_{2-x}Ce_xCuO_4$: (a) $x = 0.0$, (b) $x = 0.05$, (c) $x = 0.10$, (d) $x = 0.12$, and (e) $x = 0.15$.

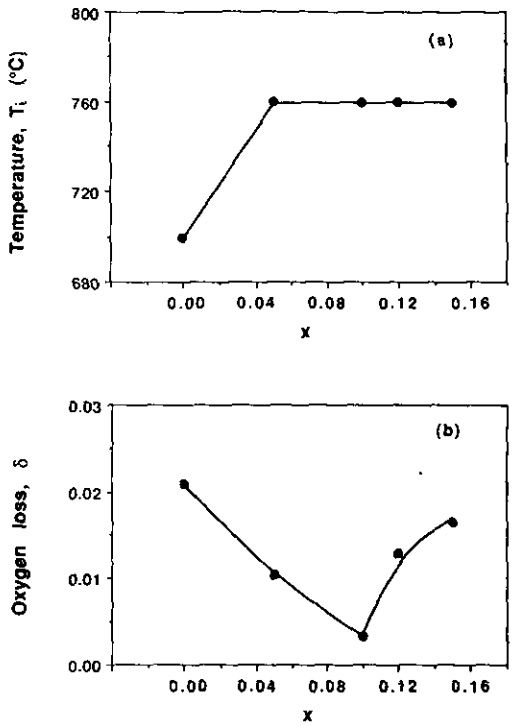

FIG. 8. Variation with x of (a) the temperature T_i at which oxygen loss begins and (b) the total amount of oxygen lost before decomposition begins for $Gd_{2-x}Ce_xCuO_4$ in N_2 atmosphere.

3.3 $Gd_{2-x}Ce_xCuO_4$ Phases

$Gd_{2-x}Cu_xCuO_4$ phases are formed for $0 \leq x \leq 0.15$ (6, 10, 23, 24); For $x > 0.15$, a $Gd_2Cu_2O_5$ impurity phase is formed. A smaller Gd^{3+} size limits the Ce solubility to 0.15. The TGA plots of $Gd_{2-x}Ce_xCuO_4$ recorded in N_2 atmosphere under identical conditions are shown in Fig. 7 for different values of x. This system is near the lower limit of the T′ phase field and several interesting observations are found.

The temperature T_i at which oxygen loss begins increases from 700°C at $x = 0$ to 760°C at $x = 0.05$, and remains constant thereafter (Fig. 8a). The phases all begin to disproportionate in the temperature range $905 \leq T \leq 920°C$ into Gd_2O_3, CeO_2, and Cu_2O as indicated by a sharp

weight loss as well as an X-ray diffraction analysis of the products. Below the decomposition temperature, the oxygen loss occurs smoothly in one step for $x = 0.0$ as in the case of $Nd_{1.85}Ce_{0.15}CuO_4$, but in two steps for $0.05 \leq x \leq 0.15$ as in the case of $Eu_{1.85}Ce_{0.15}CuO_4$ (Fig. 5). The first loss in the temperature range $760 \leq T \leq 800$°C corresponds to the removal of interstitial oxygen atoms from the octahedral sites. The second loss, if any, in the temperature range $800 \leq T \leq 920$°C corresponds to the removal of oxygen atoms from the tetrahedral sites. The first loss becomes more pronounced as the value of x increases, while the second loss becomes less pronounced, i.e., the amount of oxygen lost from octahedral interstitial sites increases with x, while that from tetrahedral sites decreases with x at least in the range $0.05 \leq x \leq 0.12$. The second loss is not observed for $x = 0.10$ and 0.12, but the end member with $x = 0.15$ seems to have a small second loss. The total amount of oxygen lost below the decomposition temperature $T \leq 920$°C is plotted as a function of x in Fig. 8b. It decreases with x in the range $0.0 \leq x \leq 0.10$ and increases again in the range $0.12 \leq x \leq 0.15$.

We now turn to a discussion of the above results. The initial increase in T_i in Fig. 8, as well as the decreasing tendency to lose oxygen from the tetrahedral sites, are due to the decreasing internal stresses with increasing Ce content. The decrease in the total amount of oxygen lost with x in the range $0.0 \leq x \leq 0.10$ is also in accordance with this expectation. Although a decreasing degree of internal stresses would be expected to increase T_i with increasing x, T_i remains constant at 760°C for $0.05 \leq x \leq 0.15$. This is because a larger electrostatic repulsion between the tetrahedral- and octahedral-site oxygen atoms—originating from a smaller lattice parameter $a \approx 3.90$ Å—forces the interstitial oxygen atoms to be lost at a lower T_i.

The increase in the amount of octahedral interstitial oxygen with x needs further consideration. The system $Gd_{2-x}Ce_xCuO_4$ is near the lower limit of the T′ phase field and the internal stresses are relatively lower (Table 2). Near the solubility limit $x = 0.15$, the tensile stress in the Cu–O bonds and the compressive stress in the (Gd, Ce)–O bonds may all be relieved at the synthesis temperature $T \approx 1000$°C. However, as the sample is cooled from the synthesis temperature, a small amount of compressive stress in the Cu–O bonds and tensile stress in the (Gd, Ce)–O bonds may set in due to a larger thermal contraction of the more ionic (Gd, Ce)–O bonds compared to that of the less ionic Cu–O bonds (8). These internal stresses can be relieved by accommodating excess interstitial oxygen atoms in the octahedral sites at lower temperatures similar to that found in the tetrahedral interstitial sites of $La_2CuO_{4+\delta}$ (25–27). But the electrostatic repulsion between the tetrahedral- and octahedral-site oxygen atoms, arising from the smaller a lattice parameters of the system $Gd_{2-x}Ce_xCuO_4$, will oppose the accommodation of interstitial oxygen atoms. The tendency to accommodate on cooling interstitial oxygen atoms will, therefore, increase with x due to an increasing compressive stress in the Cu–O bonds. This is reflected in an increase of interstitial oxygen atoms with x (Fig. 7). The increase in interstitial oxygen could also reduce the Cu^+ concentration arising from an increasing Ce content. The increasing interstitial oxygen atoms with x results in a reversal of the trend of total oxygen lost (Fig. 8b) near the solubility limit $0.12 \leq x \leq 0.15$.

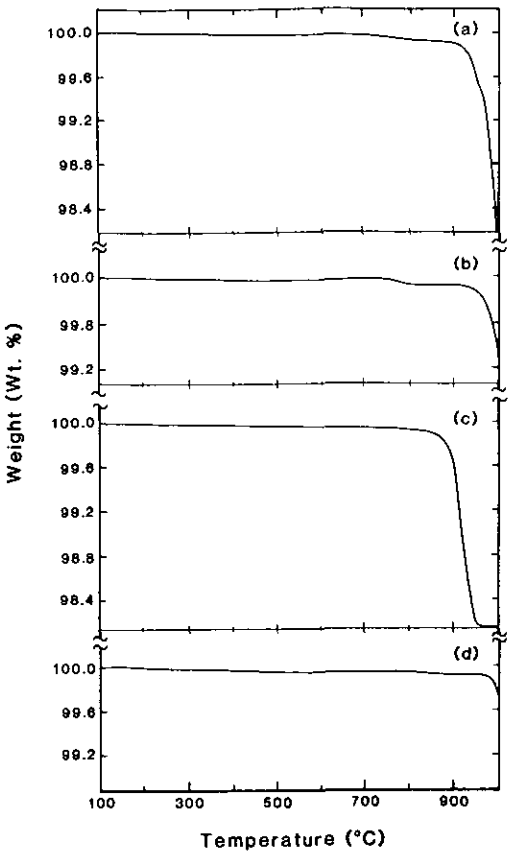

FIG. 9. Comparison of the TGA plots recorded in N_2 atmosphere for (a) Gd_2CuO_4, (b) $Gd_{1.85}Ce_{0.15}CuO_4$, (c) $Gd_{1.4}Dy_{0.6}CuO_4$, and (d) $GdDy_{0.9}Ce_{0.10}CuO_4$.

The temperature at which $Gd_{2-x}Ce_xCuO_4$ phases begin to decompose increases slightly with x; it increases from 905°C at $x = 0.0$ to 920°C at $x = 0.15$. Also the temperature at which decomposition completes increases with x. The decomposition is complete at 1000°C for $x = 0$, as indiated by a flattening of the TGA curve, but at progressively higher temperatures for $x > 0$ (Fig. 9). This conclusion is also supported by an X-ray diffraction analysis of the products obtained after performing the TGA experiment

to 1000°C. The $x = 0$ sample showed reflections due to only Gd_2O_3 and Cu_2O while the samples with $x \geq 0.05$ showed reflections due to undecomposed $Gd_{2-x}Ce_xCuO_4$ in addition to Gd_2O_3, CeO_2, and Cu_2O; the amount of undecomposed $Gd_{2-x}Ce_xCuO_4$ increased with x. The smaller Ce^{4+} ions seem to bond more strongly to the O^{2-} ions and increase marginally the phase stability.

We also compare in Fig. 9 the TGA plots of $Gd_{1.4}Dy_{0.6}CuO_4$ and $GdDy_{0.9}Ce_{0.1}CuO_4$ with those of Gd_2CuO_4 and $Gd_{1.85}Ce_{0.15}CuO_4$. $Gd_{1.4}Dy_{0.6}CuO_4$ represents the lowest limit for the T′ phase field and decomposes at a lower temperature than Gd_2CuO_4, as one would expect from decreasing size of Ln^{3+}. Incorporation of Ce into $GdDy_{0.9}Ce_{0.1}CuO_4$ increases the phase decomposition temperature similar to that in $Gd_{1.85}Ce_{0.15}CuO_4$.

4. CONCLUSIONS

The variation of oxygen loss with Ce content and the size of Ln^{3+} has been investigated systematically by TGA and the results are summarized below:

1. With increasing Ce content in $LaNd_{1-x}Ce_xCuO_4$ or decreasing Ln^{3+} size in $Ln_{2-x}Ce_xCuO_4$ for $Ln = (La_{1-y}Nd_y)$ and Nd, the temperature at which oxygen loss begins increases and the amount of loss at a given temperature $T \approx 1000$°C decreases due to a decreasing degree of internal stresses. The strain in the Cu–O bond calculated from bond valence sum is in support of this observation.

2. The oxygen loss occurs in a smooth single step for larger Ln = (La, Nd), Nd, and Sm, but in two distinct steps for smaller Ln = Eu or Gd. An increasing electrostatic repulsion between the oxygen atoms in the octahedral interstitial and tetrahedral sites forces the interstitial oxygen atoms to be lost at lower temperatures in the latter cases.

3. A smooth single-step loss for larger Ln seems to indicate that the difference in activation energies for the removal of oxygen atoms from the octahedral interstitial and the tetrahedral sites is small.

ACKNOWLEDGMENTS

Financial support by the Robert A. Welch Foundation Grant F-1254 and the National Science Foundation Grant DMR-9223552 is gratefully acknowledged.

REFERENCES

1. J. B. Goodenough, *Supercond. Sci. Technol.* **3,** 26 (1990).
2. J. B. Goodenough and A. Manthiram, *J. Solid State Chem.* **88,** 115 (1990).
3. I. D. Brown, *J. Solid State Chem.* **82,** 122 (1989).
4. I. D. Brown, *J. Solid State Chem.* **90,** 155 (1991).
5. J. P. Zhou, D. R. Riley, and J. T. McDevitt, *Chem. Mater.* **5,** 361 (1993).
6. Y. T. Zhu and A. Manthiram, *Phys. Rev. B* **49,** 6293 (1994).
7. E. Takayama-Muromachi, Y. Uchida, and K. Kato, *Physica C* **165,** 147 (1990).
8. A. Manthiram and J. B. Goodenough, *J. Solid State Chem.* **92,** 231 (1991).
9. A. Manthiram, *J. Solid State Chem.* **100,** 383 (1992).
10. A. Manthiram and Y. T. Zhu, *J. Electron. Mater.* **22,** 1195 (1993).
11. Y. T. Zhu and A. Manthiram, *Physica C* **224,** 256 (1994).
12. E. Moran, A. I. Nazzal, T. C. Huang, and J. B. Torrance, *Physica C* **160,** 30 (1989).
13. P. W. Klamut, *J. Alloys Compounds* **194,** L5 (1993).
14. E. Wang, J. M. Tarascon, L. H. Greene, and G. W. Hull, *Phys. Rev. B* **41,** 6582 (1990).
15. E. Takayama-Muromachi, F. Izumi, Y. Uchida, K. Kato, and S. Asano, *Physica C* **159,** 634 (1990).
16. I. D. Brown and D. Altermatt, *Acta Crystallogr. Sect. B* **41,** 244 (1985).
17. I. D. Brown and R. D. Shannon, *Acta Crystallogr. Sect. A* **29,** 266 (1973).
18. I. D. Brown, *Chem. Soc. Rev.* **7,** 359 (1978).
19. J. Koehler and A. Simon, *Angew. Chem. Int. Ed. Engl.* **25,** 996 (1986).
20. J. J. Capponi, C. Chaillout, A. W. Hewat, P. Lejay, M. Marezio, N. Nguyen, B. Raveau, J. L. Soubeyroux, J. L. Tholence, and R. Tournier, *Europhys. Lett.* **3,** 1301 (1987).
21. A. W. Hewat, J. J. Capponi, C. Chaillout, M. Marezio, and E. A. Hewat, *Solid State Commun.* **64,** 301 (1987).
22. W. I. F. David, W. T. A. Harrison, J. M. F. Gunn, O. Moze, A. K. Soper, P. Day, J. D. Jorgensen, D. G. Hinks, M. A. Beno, L. Soderholm, D. W. Capone, II, I. K. Shuller, C. U. Segre, K. Zhang, and J. D. Grace, *Nature (London)* **327,** 310 (1987).
23. T. C. Huang, E. Moran, A. I. Nazzal, and J. B. Torrance, *Physica C* **158,** 148 (1989).
24. Y. K. Tao, M. Bonvalot, Y. Y. Sun, R. L. Meng, P. H. Hor, and C. W. Chu, *Physica C* **165,** 13 (1990).
25. J.-S. Zhou, S. Sinha, and J. B. Goodenough, *Phys. Rev. B* **39,** 12,331 (1988).
26. J. D. Jorgensen, B. Dabrowski, Shiyou Pei, D. G. Hinks, and L. Soderholm, *Phys. Rev. B* **38,** 11,337 (1988).
27. C. Chaillout, S. W. Cheong, Z. Fisk, M. S. Lehman, M. Marezio, B. Morosin, and J. E. Schirber, *Physica C* **158,** 183 (1989).